

Complete solution for strain-induced pseudo vector potentials in graphene

Alexander L Kitt,¹ Vitor M. Pereira,² Anna K Swan,^{3,1,4} and Bennett B Goldberg^{1,5,4,*}

¹*Department of Physics, Boston University, 590 Commonwealth Ave, Boston, Massachusetts 02215, USA*

²*Graphene Research Centre and Department of Physics,*

National University of Singapore, 2 Science Drive 3, Singapore 117542

³*Department of Electrical and Computer Engineering,*

Boston University, 8 St Mary's St, Boston, Massachusetts 02215, USA

⁴*Photonics Center, Boston University, 8 St Mary's St, Boston, Massachusetts 02215, USA*

⁵*Center for Nanoscience, Boston University, 8 St Mary's St, Boston, Massachusetts 02215, USA*

Previously, certain applied strains in graphene have been shown to generate pseudo magnetic fields. Here we show that by including the lattice deformations in a tight binding model of strained graphene, new leading order terms in the strain-induced pseudo vector potential are found. These terms remove the K point symmetry of earlier solutions, causing each population of electrons to feel different pseudo magnetic fields. Isotropic strain, a case where the pseudo vector potential is solely determined by the lattice deformation, is used to illustrate the conceptual importance of the new terms. Finally, it is demonstrated that these additional terms will force reconsideration of the strain geometries that were previously thought to generate particular pseudo magnetic fields.

PACS numbers: 81.05.eu, 73.22.Pr, 71.70.Di, 85.35.-p

Many surprising properties of graphene can be engineered to create novel physical effects: The linear energy dispersion and coherent electrons near the Fermi energy can create Klein tunneling[1] and Veselago lenses[2], the latter from doping with applied electrical fields; the Dirac-like dispersion in combination with applied magnetic fields results in relativistic spacing of Landau level quantization, visible even at room temperature[3]. Graphene is also an extremely strong material with an effective Young's modulus of 1 TPa and an intrinsic strength of 130 GPa[4]. Recently, quantized Landau-like levels were observed in scanning tunneling spectroscopy in the absence of an external magnetic field[5]. This behavior has been explained in terms of a strain-induced pseudo vector potential caused by bubbles of graphene on Pt, effectively creating a pseudo magnetic field of 300 T [6, 7]. Such pseudo fields can be used for strain engineered electron confinement and collimation applications, representing a unique crossover between the unusual mechanical and electronic properties of graphene[8].

However, prior works considered only the change in the nearest neighbor hopping energy when deriving the pseudo vector potential. Here we show that including lattice deformations introduces new terms of the same order in strain as the nearest neighbor hopping, with the result that pseudo vector potential is different at each K point, causing each population of electrons to feel different strain-induced pseudo magnetic fields. We use isotropic strain, a situation where lattice deformations solely determine the pseudo vector potential, to illustrate the conceptual importance of these new terms. Finally, we exhibit how the additional terms force us to rethink the strain geometries that were previously thought to generate particular pseudo magnetic fields.

The band structure of graphene was first calculated

in 1947 by PR Wallace using a nearest neighbor tight binding formalism [9] and is characterized by two energy bands which touch at the 6 corners of the hexagonal Brillouin zone. The dispersion is linear near these points giving them their name, Dirac points, after the relativistic Dirac fermions that occupy them. For undoped graphene, the Fermi energy sits at the Dirac points. For unstrained graphene, the Dirac points form two equivalent sets of three, referred to as K and K'.

Pereira, Castro Neto, and Peres generalized the tight binding Hamiltonian to include strain and found that uniaxial strain shifts the Dirac points [10]. They emphasized the need to account for the change in nearest neighbor hopping energy as well as the lattice deformation when including strain in the Hamiltonian. The lattice deformation effect on the nearest neighbor vector is illustrated in figure 1, where the black dots represent the positions of the unstrained nearest neighbors, and the grey dots represent the position of the strained nearest neighbors under 20 % uniaxial strain in the armchair direction. The length and direction of the three unstrained nearest neighbor vectors $\vec{\delta}_i$ becomes $\vec{\delta}'_i = (I + \epsilon)\vec{\delta}_i$ under strain, where I is the identity matrix and ϵ is the two dimensional strain tensor in Cartesian coordinates, with the x axis in the armchair direction.

A closed form solution for the shift of the Dirac points due to strain can be found by approximating the strain-altered Hamiltonian near the K points. By shifting the Dirac points, strain shifts the momentum of the electrons at the Fermi level. This shift is analogous to the shift of an electron's canonical momentum due to a magnetic field $\vec{p}_{con} = m\vec{v} + q\vec{A}$ where $\vec{\nabla} \times \vec{A} = \vec{B}$. Thus, the strain-induced shift of the Dirac points, $\Delta\vec{k}_D$ can be identified as a pseudo vector potential $\vec{A} = -\frac{\hbar}{e}\Delta\vec{k}_D$.

Earlier work on carbon nanotubes [11, 12] and strained

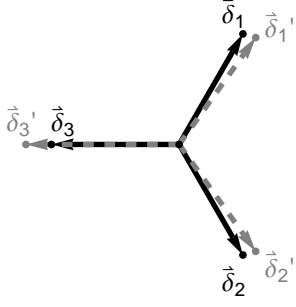


FIG. 1. The positions of the unstrained (black, dots) and strained (gray dots) nearest neighbors with the unstrained $\vec{\delta}_i$ and strained $\vec{\delta}'_i$ nearest neighbor vectors for 20 % uniaxial strain in the armchair direction. (Color online)

graphene [6, 7, 13] noted this pseudo vector potential analogy to the strain-induced shift in the Dirac points. However, these calculations neglected the lattice deformation, accounting only for the changes in nearest neighbor hopping energy. In this letter we show the importance of including *both* the lattice deformation and changes in nearest neighbor hopping when calculating the pseudo vector potential.

To derive the pseudo vector potential we start by considering the real space, nearest neighbor, tight binding Hamiltonian for the strained graphene lattice:

$$H = - \sum_{\langle i,j \rangle} t_{ij} (a_i^\dagger b_j + hc)$$

here the sum is over all nearest neighbor pairs, a_i^\dagger is the

creation operator for an electron on the A sublattice, b_j is the annihilation operator for an electron on the B sublattice, and t_{ij} is the hopping energy which is dependent on the i, j ion-ion separation l_{ij} as $t_{ij} = t_0 e^{\beta(l_{ij}/a_0 - 1)}$ with a_0 and t_0 the unstrained nearest neighbor separation and hopping energies respectively and $\beta \approx -3$ [10, 14]. The influence of the strain-induced change in hopping energy on the Hamiltonian is immediately evident. The second strain effect subtly manifests itself when changing to reciprocal space. For transparency, the phases of the Fourier transforms are selected such that the creation/annihilation operators are transformed about their respective lattice deformed sub-lattice positions [15].

$$a_i^\dagger = \frac{1}{\sqrt{N}} \sum_{\vec{k}} e^{i\vec{k} \cdot \vec{R}'_i} a_{\vec{k}}^\dagger$$

$$b_j = \frac{1}{\sqrt{N}} \sum_{\vec{k}'} e^{i\vec{k}' \cdot (\vec{R}'_j + \vec{\delta}'_j)} b_{\vec{k}'}$$

where \vec{R}'_i are the strain modified positions of the A sublattice. The resulting Hamiltonian is dependent on both the lattice deformation and the change in hopping energies due to strain

$$H = - \sum_{j=1}^3 (t_j a_k^\dagger b_{\vec{k}} e^{-i\vec{k} \cdot \vec{\delta}'_j} + hc) \quad (1)$$

We use this exact, nearest neighbor tight binding solution as a standard to which the derived pseudo vector potential is compared. When the hopping energy is expressed as $t_j = t_0 + \delta t_j$ with $\delta t_j = \mathcal{O}(\epsilon)$, the Hamiltonian can be linearized to first order in strain,

$$H = - \sum_j (t_0 e^{-i\vec{k} \cdot \vec{\delta}_j} a_k^\dagger b_{\vec{k}} + hc) - \sum_j (\delta t_j e^{-i\vec{k} \cdot \vec{\delta}_j} a_k^\dagger b_{\vec{k}} + hc) + i \sum_j (t_0 \vec{k} \cdot \epsilon \vec{\delta}_j e^{-i\vec{k} \cdot \vec{\delta}_j} a_k^\dagger b_{\vec{k}} + hc) + \mathcal{O}(\epsilon^2) \quad (2)$$

The first term is the unstrained Hamiltonian, the second term is due to the changes in the hopping energies, and the third term is the new term due to the lattice deformation. The dependence of δt_j on strain is taken from Castro Neto et al [6] except here we take $\kappa = 1$ because the atomic displacements due to elastic strain dominate those due to optical phonons. Approximating this Hamiltonian near the six K points recovers the unstrained Hamiltonian shifted by $\Delta \vec{k}_D$. Relating this shift in the position of the Dirac points to the pseudo vector potential and defining the x axis in the arm chair direc-

tion yields the pseudo vector potential for general strain:

$$\vec{A}_{K_1} = -\vec{A}_{K'_1} = \frac{\phi_0}{a} \left(\frac{\frac{4}{3\sqrt{3}}\epsilon_{xy}}{\frac{4}{3\sqrt{3}}\epsilon_{yy}} \right) + \vec{A}_p$$

$$\vec{A}_{K_2} = -\vec{A}_{K'_2} = \frac{\phi_0}{a} \left(\frac{\frac{2}{3}\epsilon_{xx} - \frac{2\sqrt{3}}{9}\epsilon_{xy}}{\frac{2}{3}\epsilon_{xy} - \frac{2\sqrt{3}}{9}\epsilon_{yy}} \right) + \vec{A}_p$$

$$\vec{A}_{K_3} = -\vec{A}_{K'_3} = \frac{\phi_0}{a} \left(\frac{-\frac{2}{3}\epsilon_{xx} - \frac{2\sqrt{3}}{9}\epsilon_{xy}}{-\frac{2}{3}\epsilon_{xy} - \frac{2\sqrt{3}}{9}\epsilon_{yy}} \right) + \vec{A}_p$$

$$\vec{A}_p = \frac{\phi_0}{a} \left(\frac{\frac{\beta}{2\pi}\epsilon_{xy}}{\epsilon_{xx} - \epsilon_{yy}} \right) \quad (3)$$

where $\phi_0 = \frac{\pi\hbar}{e}$ is the flux quantum and the K points are defined in figure 2a. It should be noted that the strain

induced scalar potential, a second nearest neighbor effect, is unchanged by the inclusion of lattice deformations.

A limitation of prior calculations of the pseudo vector potential is that only \vec{A}_p appears in the solution above, and as a result, predict that the pseudo vector potential is the same at each of the three Dirac K points. In figure 2b we plot the band structure contours about each of the K points for 1 % isotropic, tensile strain calculated using equation 1. Overlayed on each plot are the lines depicting the strained (black, solid) and un-strained (red, dashed) Brillouin zone boundaries. The increase in the lattice size yields a decrease in the size of the Brillouin Zone. For this case of isotropic strain, the symmetry of the strained lattice is conserved, causing the Dirac points to stay pinned to the corners of the Brillouin zone. As a result, and distinct from prior work, each Dirac point shifts in toward the Γ point resulting in a different directional shift (no valley symmetry) at each K point. Further, since $\vec{A}_p = 0$ for isotropic strain, considering only this term results in missing the actual strain-induced shift of the Dirac points, now correctly accounted for in the new terms in equation 3. The shift in the Dirac point predicted by these new terms is plotted as the orange arrow in figure 2b. Similar plots for shear strain and for uniaxial strain in the zig zag and armchair directions are included in the supplemental material (supplemental material included after references).

The analogy between the shift in the Dirac points and the vector potential in electricity and magnetism is not perfect. Unlike a magnetic field, strain does not break time reversal symmetry. This is manifest in the sign change between the pseudo vector potential at each K point and its time reversal pair [6] as seen in equation 3. Additionally, the pseudo vector potential does not have Gauge freedom because it is directly determined by a measurable. Even so, the pseudo vector potential can exhibit Landau level quantization and so when considering device designs to measure strain-induced Landau quantization it is important to note that the pseudo vector potential is dependent on the crystallographic orientation of the strain as demonstrated here.

With a clear and complete understanding of the creation of the pseudo vector potential due to the application of strain, we now turn to the resulting pseudo magnetic field. The pseudo magnetic field is truly pseudo; strain does not create a real magnetic field. Nonetheless, the electrons form relativistic Landau levels as if they were in a perpendicular magnetic field determined by the particular valley, given by $\vec{B}_{K_i} = \nabla \times \vec{A}_{K_i}$. We treat the system as three independent populations of electrons which feel different magnetic fields.

With the theory developed above, the pseudo magnetic fields can be calculated for any given strain distribution. Prior works that accounted only for \vec{A}_p in the pseudo vector potential investigated the pseudo magnetic field created by a variety of different strain distributions [16–

22]. However, including the new terms in the pseudo vector potential drastically alters the predicted pseudo magnetic fields.

As an example, we consider graphene covering an equilateral triangular hole with a uniformly distributed out-of-plane load causing strain in the graphene membrane. This geometry was originally proposed by Guinea, Katnelson, and Geim as a simple method of generating fairly uniform pseudo magnetic fields [18]. We calculate the strain fields using finite element analysis to determine the pseudo vector potentials at each element and then numerically differentiate to determine the local pseudo magnetic fields. The finite element analysis was performed using Comsol Multiphysics with a two-dimensional thin plate model including geometric non-linearity. The edges were fixed and the pressure was applied using a face load. Graphene's Young's Modulus of 1 TPa and thickness of 3.5 Angstroms [4] were used along with the Poisson ratio of graphite of 0.165 [4, 24]. To make the triangles more realistic we include 2 nm radius fillets on the three corners. The surface was meshed with triangles with a maximum element size of 1 nm. The strain fields were evaluated in the mid-plane of the plate.

The effect of the new terms in the pseudo vector potential on the predicted pseudo magnetic field is shown in figure 3 for an equilateral triangle with 50 nm sides under 14 MPa of pressure. Figure 3a shows the results of calculations performed using only \vec{A}_p in the pseudo vector potential resulting in a fairly uniform pseudo magnetic field in agreement with Guinea, Katnelson, and Geim. In comparison, figures 3b and 3c demonstrate that the new terms in the pseudo vector potential cause the electrons at the three different K points to experience drastically different pseudo magnetic fields, obviating the uniformity which originally made this device design useful. It is clear that the corrections to the pseudo vector potential require us to rethink the methods for creating large and uniform pseudo magnetic fields. We note that the differences in the pseudo magnetic fields at the different K points may, however, be extremely useful in valleytronics [25].

In this letter we have shown that by neglecting the strain-induced lattice deformation when deriving the pseudo vector potential, past calculations have missed an important leading order term. This term has a different form at each K point, a result that we showed was necessary to explain the shift of the Dirac peaks due to isotropic strain. Finally, using the example of a graphene covered equilateral triangular hole under external pressure we showed how the additional terms require us to rethink previously proposed methods for generating particular magnetic fields.

VMP acknowledges supported by the NRF-CRP award "Novel 2D materials with tailored properties: beyond graphene" (R-144-000-295-281).

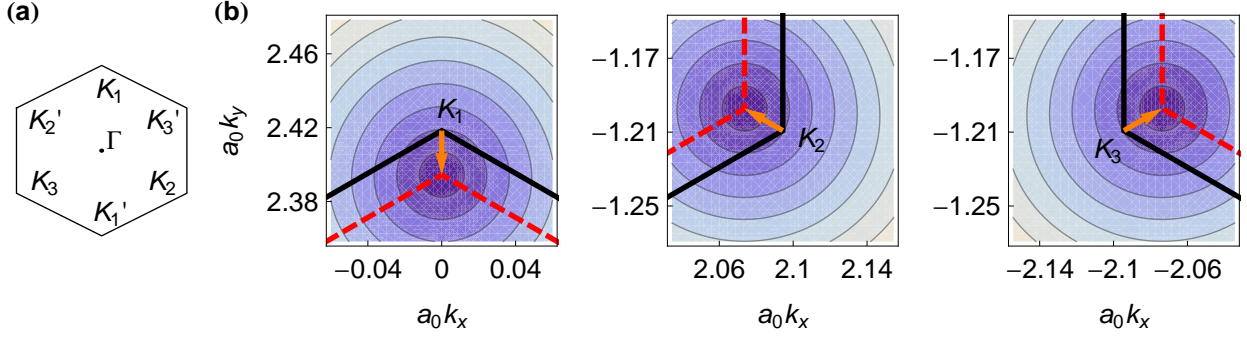


FIG. 2. (a) The unstrained Brillouin zone of graphene with labeled high symmetry points (b) Contours of the band structure of graphene under 1% tensile isotropic strain near the three K points overlaid with the Brillouin zone of the unstrained graphene (solid, black) and the strained graphene (dashed, red), as well as the shift in the Dirac points predicted by equation 3 (orange, arrow). (Color online)

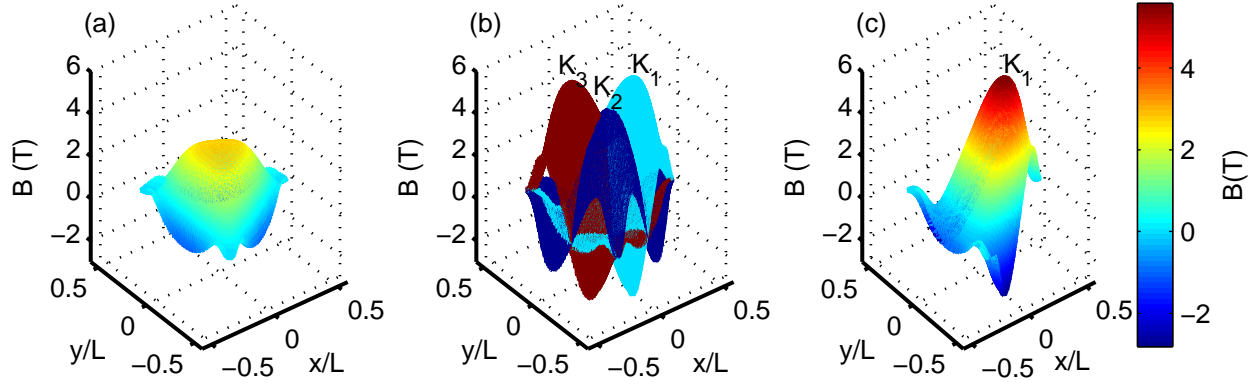


FIG. 3. The spatial distribution of the pseudo magnetic fields generated when an equilateral triangle with 50 nm sides, 2 nm radius fillets, and the base oriented 30 degrees CCW from the armchair direction is pressurized to 14 MPa. In (a) the calculation is done using only \vec{A}_p in equation 3, while in (b) it is done including the newly derived terms. Here, the three different colored curves correspond to the pseudo magnetic fields felt by the electrons at the three different K points with the magnetic field for the electrons at K_1 isolated (c). (Color online)

* goldberg@bu.edu

- [1] C. Beenakker, Reviews of Modern Physics **80**, 1337 (2008), ISSN 0034-6861, URL <http://link.aps.org/doi/10.1103/RevModPhys.80.1337>.
- [2] V. Cheianov, V. Fal'ko, and B. Altshuler, Science **315**, 1252 (2007), ISSN 1095-9203, URL <http://www.sciencemag.org/cgi/doi/10.1126/science.1138020>.
- [3] K. Novoselov, Z. Jiang, Y. Zhang, S. Morozov, H. Stormer, U. Zeitler, J. Maan, G. Boebinger, P. Kim, and A. Geim, Science **315**, 1379 (2007), ISSN 1095-9203, URL <http://www.sciencemag.org/cgi/doi/10.1126/science.1137201>.
- [4] C. Lee, X. Wei, J. Kysar, and J. Hone, Science **321**, 385 (2008), ISSN 1095-9203, URL <http://www.sciencemag.org/cgi/doi/10.1126/science.1157996>.
- [5] N. Levy, S. Burke, K. Meaker, M. Panlasigui, A. Zettl, F. Guinea, A. Castro Neto, and M. Crommie, Science **329**, 544 (2010), ISSN 0036-8075, URL <http://www.sciencemag.org/cgi/doi/10.1126/science.1191700>.
- [6] A. Castro Neto, F. Guinea, N. Peres, K. Novoselov, and A. Geim, Reviews of Modern Physics **81**, 109 (2009), ISSN 0034-6861, URL <http://link.aps.org/doi/10.1103/RevModPhys.81.109>.
- [7] M. Vozmediano, M. Katsnelson, and F. Guinea, Physics Reports **496**, 109 (2010), ISSN 0370-1573, URL <http://linkinghub.elsevier.com/retrieve/pii/S0370157310001729>.
- [8] V. Pereira and A. Castro Neto, Physical Review Letters **103**, 046801 (2009), ISSN 0031-9007, URL <http://link.aps.org/doi/10.1103/PhysRevLett.103.046801>.
- [9] P. Wallace, Physical Review **71**, 622 (1947), URL <http://link.aps.org/doi/10.1103/PhysRev.71.622>.
- [10] V. Pereira, A. Castro Neto, and N. Peres, Physical Review B **80**, 045401 (2009), ISSN 1098-0121, URL <http://link.aps.org/doi/10.1103/PhysRevB.80.045401>.

- [11] K. Sasaki, Y. Kawazoe, and R. Saito, Progress of Theoretical Physics **113**, 463 (2005), ISSN 0033-068X, URL <http://ptp.ipap.jp/link?PTP/113/463/>.
- [12] T. Ando, Journal of the Physical Society of Japan **75**, 124701 (2006), ISSN 0031-9015, URL <http://jpsj.ipap.jp/link?JPSJ/75/124701/>.
- [13] J. Mañes, Physical Review B **76**, 045430 (2007), ISSN 1098-0121, URL <http://link.aps.org/doi/10.1103/PhysRevB.76.045430>.
- [14] R. Ribeiro, V. Pereira, N. Peres, P. Briddon, and A. Castro Neto, New Journal of Physics **11**, 115002 (2009), ISSN 1367-2630, URL <http://stacks.iop.org/1367-2630/11/i=11/a=115002?key=crossref.265cffe8156127129572b51312612ec9>.
- [15] C. Bena and G. Montambaux, New Journal of Physics **11**, 095003 (2009), ISSN 1367-2630, URL <http://stacks.iop.org/1367-2630/11/i=9/a=095003?key=crossref.9bfc13536183dccc2af45d7976ca319>.
- [16] M. Fogler, F. Guinea, and M. I. Katsnelson, Physical Review Letters **101**, 226804 (2008), ISSN 0031-9007, URL <http://link.aps.org/doi/10.1103/PhysRevLett.101.226804>.
- [17] F. Guinea, M. Katsnelson, and M. Vozmediano, Physical Review B **77**, 075422 (2008), ISSN 1098-0121, URL <http://link.aps.org/doi/10.1103/PhysRevB.77.075422>.
- [18] F. Guinea, M. Katsnelson, and A. Geim, Nature Physics **6**, 30 (2009), ISSN 1745-2473, URL <http://www.nature.com/doi/10.1038/nphys1420>.
- [19] F. Guinea, A. Geim, M. Katsnelson, and K. Novoselov, Physical Review B **81**, 035408 (2010), ISSN 1098-0121, URL <http://link.aps.org/doi/10.1103/PhysRevB.81.035408>.
- [20] T. Low and F. Guinea, Nano Letters **10**, 3551 (2010), ISSN 1530-6992, URL <http://pubs.acs.org/doi/abs/10.1021/nl1018063>.
- [21] K. Kim, Y. Blanter, and K. Ahn, Physical Review B **84**, 081401 (2011), URL <http://link.aps.org/doi/10.1103/PhysRevB.84.081401>.
- [22] T. Low, F. Guinea, and M. Katsnelson, Physical Review B **83**, 195436 (2011), ISSN 1098-0121, URL <http://link.aps.org/doi/10.1103/PhysRevB.83.195436>.
- [23] G. Wakker, R. Tiwari, and M. Blaauboer, Physical Review B **84**, 195427 (2011), ISSN 1098-0121, URL <http://link.aps.org/doi/10.1103/PhysRevB.84.195427>.
- [24] O. Blakslee, D. Proctor, E. Seldin, G. Spence, and T. Weng, Journal of Applied Physics **41**, 3373 (1970), ISSN 00218979, URL <http://link.aip.org/link/?JAP/41/3373/1&Agg=doi>.
- [25] A. Rycerz, J. Tworzydo, and C. Beenakker, Nature Physics **3**, 172 (2007), ISSN 1745-2473, URL <http://www.nature.com/doi/10.1038/nphys547>.

SUPPLEMENTAL MATERIAL

In figure S1 the plot in figure 2 of the main text is reproduced for different strain geometries. These include uniaxial strain in the armchair direction

$$\epsilon = \begin{pmatrix} s & 0 \\ 0 & -\nu s \end{pmatrix}$$

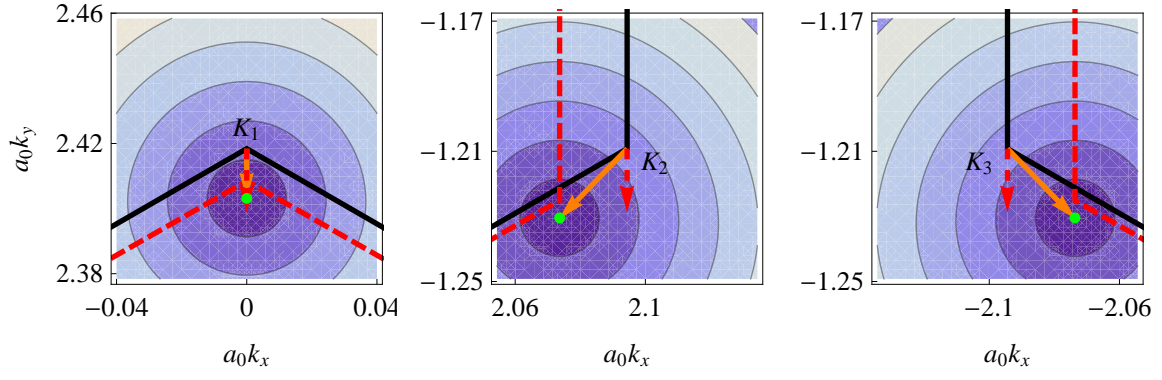
uniaxial strain in the zig direction

$$\epsilon = \begin{pmatrix} -\nu s & 0 \\ 0 & s \end{pmatrix}$$

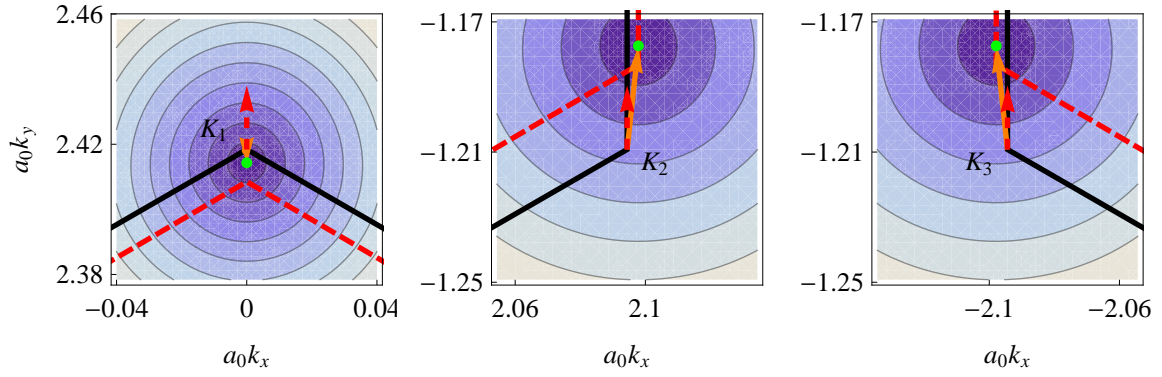
as well as pure shear strain

$$\epsilon = \begin{pmatrix} 0 & s \\ s & 0 \end{pmatrix}$$

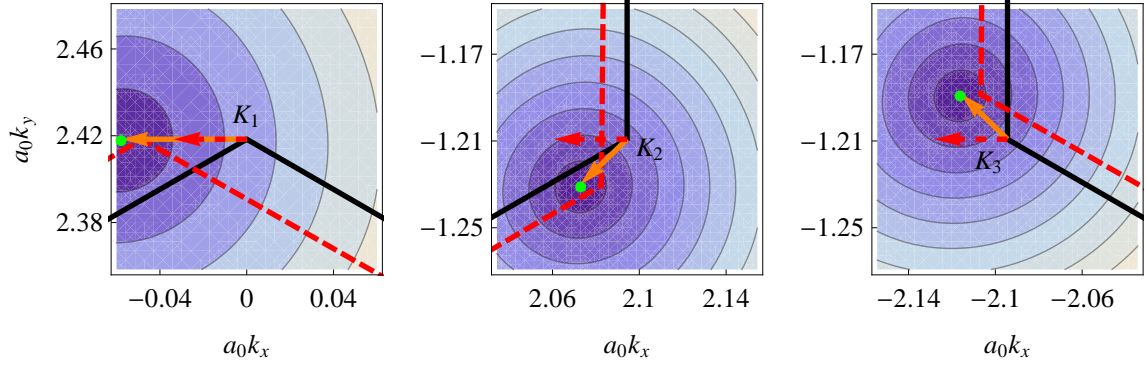
all for $s = .01$. In these cases the symmetry of the system is reduced, allowing the Dirac points to shift off of the Brillouin zone corners.



(a) Arm chair uniaxial strain



(b) Zig zag uniaxial strain



(c) Shear strain

S 1. Contours, calculated using equation 1 from the main text, of the band structure of graphene under the labeled strain conditions near the three K points overlayed with the Brillouin zone of the unstrained graphene (solid, black) and the strained graphene (dashed, red) as well as the position of the strained Dirac point (green dot) and the shift in the Dirac points predicted by equation 3 in the main text (orange, arrow).